Electronic Supplementary Material (ESI) for ChemComm.
This journal is © The Royal Society of Chemistry 2019

Electronic Supplementary Information

In Situ Formation of Nitrogen-Doped Carbon-Wrapped Co_3O_4 Enabling the Highly Efficient and Stable Catalytic Reduction of p-Nitrophenol

Experimental Procedures

Materials

All major chemicals used in our experiments were of analytical reagent grade and used without any further treatment. Cobalt chloride ($CoCl_2 \cdot 6H_2O$), sodium hydroxide (NaOH), 2,6-diaminopyridine ($C_5H_7N_3$), sodium borohydride ($NaBH_4$) and p-nitrophenol ($C_6H_5NO_3$) were purchased from Sigma-Aldrich (Shanghai, China). All experiments were carried out using deionized water produced from a Milli-Q water system (Millipore, Bedford, MA, USA).

Catalyst preparation

The Co_3O_4 was prepared according to a previously reported method.[1] Generally, 1.19 g of $CoCl_2 \cdot 6H_2O$ and 2.00 g of NaOH were dissolved into 50 mL of deionized water, respectively. After the dropwise addition of the $CoCl_2$ and NaOH aqueous solutions into a stirred three-necked flask containing 50 mL of deionized water at 50 °C under a N_2 atmosphere for 1 h, the resulting pink suspension of $Co(OH)_2$ was separated via centrifugation and washed with deionized water several times, followed by drying at 100 °C overnight. Finally, the $Co(OH)_2$ precipitate was sintered at 300 °C a ramping rate of 2 °C min^{-1} for 2 h in air to obtain the pristine Co_3O_4 material. CNx@Co_3O_4 was prepared in situ using a facile impregnation-carbonization method. After optimizing the preparing process, the best catalyst was obtained at an initial 2,6-diaminopyridine concentration of 0.83 mmol L^{-1} and carbonization temperature of 450 °C (Fig. S4). Typically, 0.1 g of Co_3O_4 was impregnated with 0.5 mL of an 0.83 mmol

L^{-1} aqueous solution of 2,6-diaminopyridine and then dried at 80 °C open to the air to obtain the precursor. Subsequently, the precursor was inserted into a tube furnace (OTF-1200X; Hefei Ke Jing Materials Technology Co., Ltd., China) and heated to a preset temperature of 450 °C under an argon atmosphere for 3 h at a heating rate of 3 °C min^{-1}. The weight percentage of CNx wrapped on the surface of Co_3O_4 was determined to be ~10% by comparing the weight difference of Co_3O_4 and CNx@Co_3O_4. As a control, a catalyst containing the same amount of CNx was loaded onto TiO_2 (CNx@TiO_2) using a similar method. The main reason for selecting TiO_2 as a support was due to the absence of interactions between the TiO_2 surface and the donor species BH_4^-.[2]

Catalytic activity

The catalytic reduction of PNP to PAP using $NaBH_4$ was performed at room temperature (25 °C) in a standard quartz cell with an operating volume of 3.5 mL. In brief, 2.0 mL of a 0.175 mmol L^{-1} aqueous solution of PNP and 0.7 mL of fresh $NaBH_4$ solution with a concentration in the range of 0.01–1.5 mol L^{-1} were added into the quartz cell. Then, 0.05 mL of a suspension containing 1 g L^{-1} of the catalyst was injected into the mixture quickly to initiate the reaction. The catalytic activity was measured using quantitative analysis of the featured absorption peaks centered at ~400 and ~300 nm for PNP and PAP, respectively using UV−visible spectroscopy (UV-2550 spectrophotometer; Shimadzu, Japan).

The initial concentrations of PNP and $NaBH_4$ were determined by dissolving

preset amounts of PNP and $NaBH_4$ in deionized water followed by adjusting the volume of solution to 25 mL using volumetric flask by the addition of deionized water, respectively. The changes in the absorbance during the $CNx@Co_3O_4$ catalyzed $NaBH_4$-PNPRR are plotted in Fig. S3. As the reaction proceeds, the maximum absorption peak corresponding to PNP at 400 nm gradually decreases, accompanied by an increase in the peak intensity at 300 nm, representing the simultaneous formation of PAP. Moreover, two isosbestic points at 277 and 320 nm can be observed, suggesting that no products other than PAP were produced.[3] According to the Lambert–Beer law, the A/A_0 value at a wavelength of 400 nm can be used to represent the ratio of the nitrophenol concentration (C) to its initial concentration (C_0).[4]

Characterization

The morphology of the catalyst was observed using transmission electron microscopy (TEM, TECNAI G2 F30 S-TWIN; FEI, USA) at an accelerating voltage of 200 kV. The Raman signal intensities of the materials were recorded on a LabRam HR800 Raman spectrometer (Horiba Jobin Yvon, France) using a 532 nm excitation laser in the wavenumber range of 20−2500 cm^{-1}. The phases present in the catalyst were determined using X-ray powder diffraction (XRD) recorded on an X-ray diffractometer (XPert Pro MPD; PANalytical B.V., Netherlands) using Cu-Kα radiation generated at 45 kV and 40 mA. The surface area was calculated using the Brunauer–Emmett-Teller (BET) method from the nitrogen adsorption and desorption isotherms recorded at 77 K using an ASAP 2010 analyzer (Micromeritics, USA). The

pore size distributions were obtained by the Barrett-Joyner-Haleda (BJH) method. The chemical composition was analyzed using X-ray photoelectron spectroscopy (XPS, Thermo ESCALAB 250XI; Thermo Fisher Scientific, USA) using an Al Kα X-ray source (hν = 1486.6 eV). The C1s (284.6 eV) peak was used to calibrate the binding energy values. The charge transfer resistance of the catalyst was verified using electrochemical impedance spectroscopy (EIS), which was recorded on a Solartron SI 1287 electrochemical interface and SI 1260 impedance/gain-phase analyzer (Solartron, USA). The measurements were performed in a 0.1 mol L^{-1} Na_2SO_4 solution with an alternating current voltage magnitude of 5 mV over a frequency range of 10^6–10^{-1} Hz in the dark.

Results and Discussion

TEM

TEM analysis was conducted to visually observe the morphology and structure of the catalysts. As shown in Fig. 1(a), pristine Co_3O_4 is regular in shape presenting a well-defined hexagonal morphology, which is in accordance with that reported in the literature.[1] The average edge length of the hexagonal nanoplates was determined to be ~60 nm. In addition, pores with diameters in the range of 5–10 nm were present in the nanoplates as a consequence of the dehydration of $Co(OH)_2$ to Co_3O_4.[5] The morphology of CNx@Co_3O_4 was different to that observed for pristine Co_3O_4 (Fig. 1(b)). The hexagonal nanoplates with pores was not maintained. The HRTEM of the insets shown in Fig. 1(a) and (b) present the lattice fringes with an interplanar spacing of 0.29 nm, which can be attributed to the (2 2 0) facets of cubic Co_3O_4, which is in good accordance with the XRD results described below. Moreover, a thin-surface CNx layer wrapping the crystalline core of Co_3O_4 can be clearly observed in the HRTEM image (inset of Fig. 1(b)). The thickness of the CNx layer was determined to be ~2 nm. As a reference, the HRTEM image of pristine Co_3O_4 (Fig. 1(a)) does not indicate the presence of a CNx layer on its surface. In addition, no obvious change in the morphology was seen on the CNx@Co_3O_4 surface after the reaction (Fig. 1(c)).

Raman analysis

Fig. 1(d) shows the Raman analysis of the CNx@Co_3O_4 with reference to Co_3O_4. Five Raman peaks in the wavenumber range from 180 to 780 cm^{-1} correspond to the

five dynamic modes of the spinel structure of cobalt oxide, including F^1_{2g}, E^2_{1g}, F^3_{2g}, F^4_{2g} and A^5_{1g}, respectively.[6] The results are in good agreement with the XRD analysis described below. A tiny blue-shift in peaks observed for CNx@Co_3O_4 relative to Co_3O_4 can be attributed to the presence of the surface oxygen vacancies in CNx@Co_3O_4.[7] In addition, when compared to Co_3O_4, the CNx@Co_3O_4 and CNx@TiO_2 samples have characteristic peaks at 1360 and 1570 cm^{-1}, corresponding to the representative Raman peaks of carbon composites.[8] The results, together with the TEM images, demonstrate the successful wrapping of CNx on Co_3O_4. The peaks at 1360 and 1570 cm^{-1} were characterized as the D (defects and disorder) and G (graphite) bands, respectively.[9] The ratio of the two peak intensities (I_D/I_G) represents the defect density in the catalyst. The I_D/I_G values were ~1.3 and ~1.2 for CNx@Co_3O_4 and CNx@TiO_2, respectively, indicating the similar structure of CNx on Co_3O_4 and TiO_2. Moreover, the I_D/I_G value was >1, which implies that the carbon is present as a disordered structure on the surface of Co_3O_4 and TiO_2.[10] The disordered structure should originate from the heteroatoms (N) in the graphite-like carbon framework as a result of the carbonization of 2,6-diaminopyridine. In addition, almost no change in the Raman spectrum recorded for CNx@Co_3O_4 was observed before and after the reaction (Fig. 1(d)), which confirm the stability of the catalyst.

XRD and N_2 physisorption

The powder XRD patterns obtained for Co_3O_4 and CNx@Co_3O_4 are displayed in Fig. 1(e). CNx@Co_3O_4 clearly exhibits a typical spinel Co_3O_4 pattern (JCPDS 42-1467)

with a cubic crystal system.[11] This result confirms that the crystal structure of pristine Co_3O_4 is well preserved after wrapping with CNx. No characteristic peaks belonging to carbon were identified in CNx@Co_3O_4, which may be attributed to the low carbon content and/or the amorphous nature of CNx.[12,13] XRD was also performed on the used CNx@Co_3O_4 catalyst. The spectrum was identical to that recorded for the pristine catalyst (Fig. 1(e)), suggesting no phase changes occurred after the reaction.

Table S1 lists the surface areas of CNx@Co_3O_4 and its reference compounds, which were calculated to be 55.4, 77.2 and 39.1 $m^2\ g^{-1}$ according to the BET method for Co_3O_4, CNx@TiO_2 and CNx@Co_3O_4, respectively. Obviously, the BET surface area of Co_3O_4 slightly decreased upon wrapping CNx onto its surface, which was attributed to the partial blockage of porosity during the fabrication process.[14] The nitrogen adsorption–desorption isotherms of Co_3O_4 and CNx@Co_3O_4 samples exhibit the characteristic Type IV adsorption isotherms, with a Type I hysteresis loop typical of a regular ordered mesoporous structure (Fig. S1(a)).[1] The BJH pore-size distribution plots (Fig. S1(b)) also clearly show Co_3O_4 and CNx@Co_3O_4 presenting well-developed mesopores (2–50 nm). The presence of mesopores allow the PNP pass through the outer CNx layer and access the inner Co_3O_4.

XPS

The chemical environment and surface elemental composition of the samples were obtained using XPS. The Co 2p spectra shown in Fig. S2(a) exhibits two peaks at 794.8 and 779.6 eV, corresponding to Co $2p_{1/2}$ and Co $2p_{3/2}$ spin-orbital peaks of Co_3O_4,

respectively. The spin-orbital doublet splitting was ~15.2 eV, confirming the presence of Co_3O_4.[15] In addition, two typical shake-up satellite peaks related to the two oxidation states of Co_3O_4 were identified. The positive shift in the binding energy value (~0.3 eV) of CNx@Co_3O_4 relative to Co_3O_4 was attributed to the interaction between the Co and N atoms.[15-17]

With respect to Co_3O_4, the N 1s XPS spectrum was observed for CNx@Co_3O_4 (Fig. S2(b)). The N 1s peak was well fitted into four peaks located at 398.3, 399.3, 400.2 and 401.1 eV, corresponding to the oxidation states of pyridinic N, Co-coordinated N, pyrrolic N and graphitic N, respectively.[6,17] The presence of Co–N bond favors electron transfer between Co_3O_4 and CNx during the catalytic $NaBH_4$-PNPRR.

The O 1s peaks observed for raw Co_3O_4 and CNx@Co_3O_4 were composed of three chemical states (Fig. S2(c)). The first peak at 529.7 eV is related to the cobalt-oxygen bonding state in the Co_3O_4 lattice (O_L), the second peak at 530.7 eV corresponds to the surface adsorbed hydroxyl groups (O_V) and the third peak at 532.2 eV can be assigned to surface adsorbed water molecules (O_A), respectively.[7,18] Among them, the intensity of the O_V peak is directly associated with the number of oxygen vacancies or defects.[7,15,18] By estimating the area that the fitted curve covers, the relative contribution of the O_V peak area increases slightly for the CNx@Co_3O_4 when compared to Co_3O_4.

The deconvoluted high-resolution C 1s XPS spectra of Co_3O_4 and CNx@Co_3O_4 are presented in Fig. S2(d). The three fitted peaks located at binding energies of 284.6, 285.6 and 288.4 eV represent the three different chemical environments of the carbon atoms.[19,20] In contrast to Co_3O_4, a new peak assigned to the CN bond was detected at

288.4 eV for CNx@Co_3O_4,[21] revealing the presence of CNx, which is in accordance with the TEM and Raman results. It should be noted that no obvious difference between the fresh and used samples can be observed (Fig. S2), indicating the excellent stability of CNx@Co_3O_4.

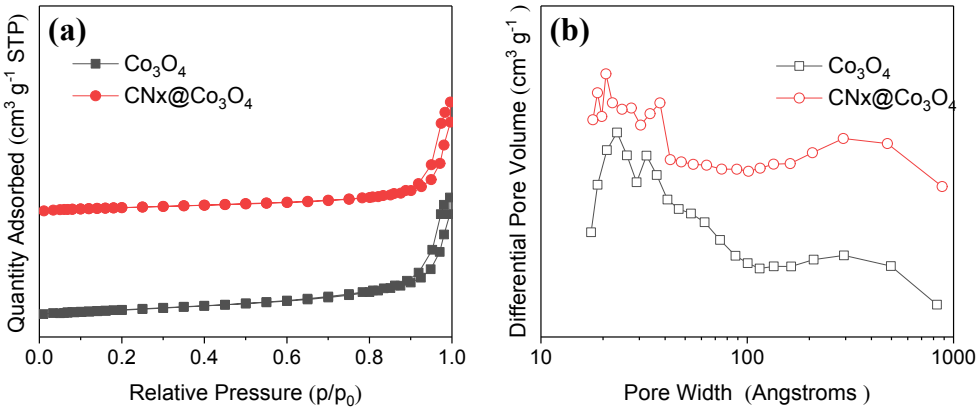

Fig. S1 Nitrogen adsorption-desorption isotherms (a) and corresponding pore-size distributions (b) of CNx@Co_3O_4 and Co_3O_4.

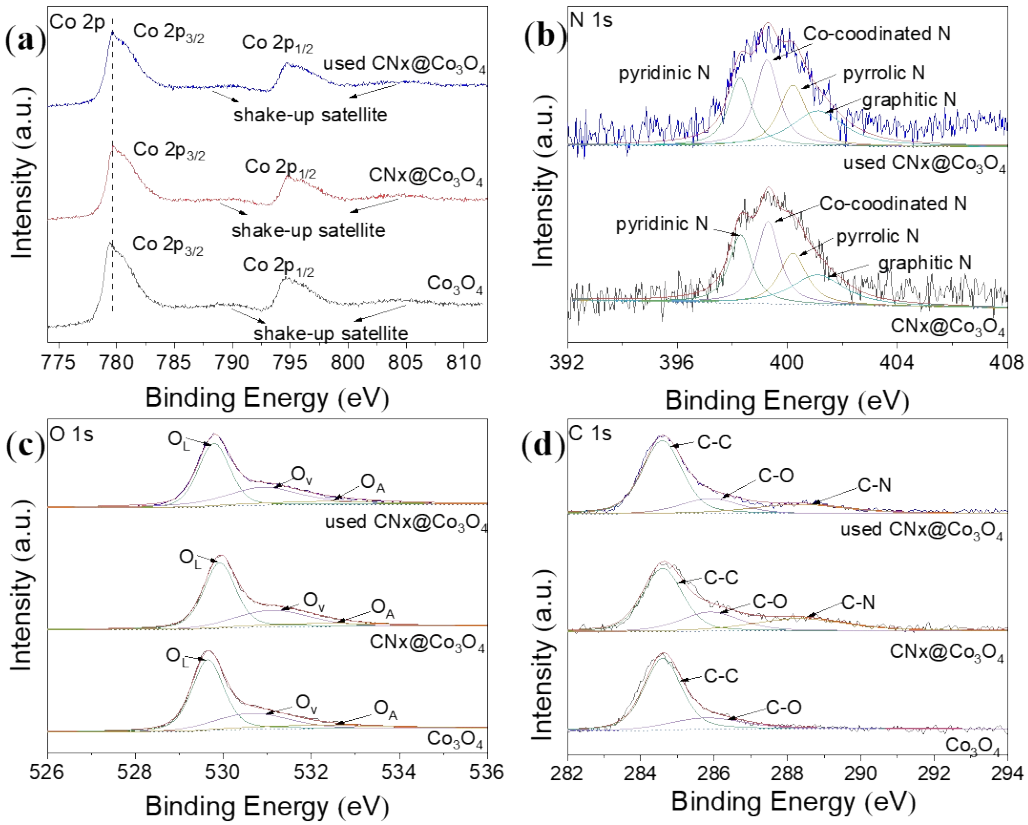

Fig. S2 The (a) Co 2p, (b) N 1s, (c) O 1s and (d) C 1s core level XPS spectra recorded for Co_3O_4, CNx@Co_3O_4 and used CNx@Co_3O_4.

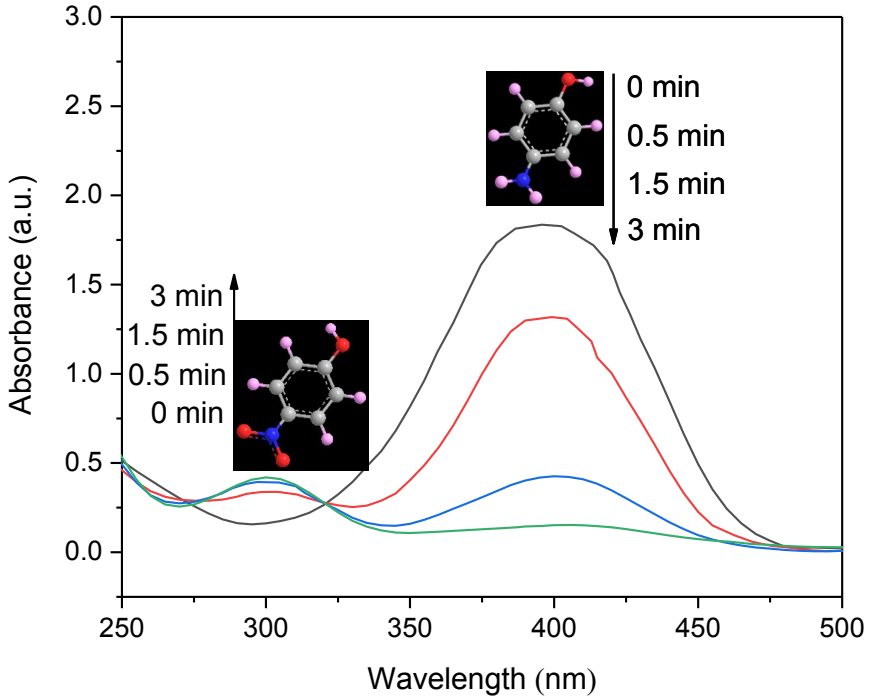

Fig. S3 Typical evolution of the UV–vis absorption spectra during the catalytic reduction of PNP using CNx@Co_3O_4. CNx@Co_3O_4 loading = 0.05 mg, initial PNP concentration = 0.13 mmol L^{-1} and initial $NaBH_4$ concentration = 0.013 mol L^{-1}.

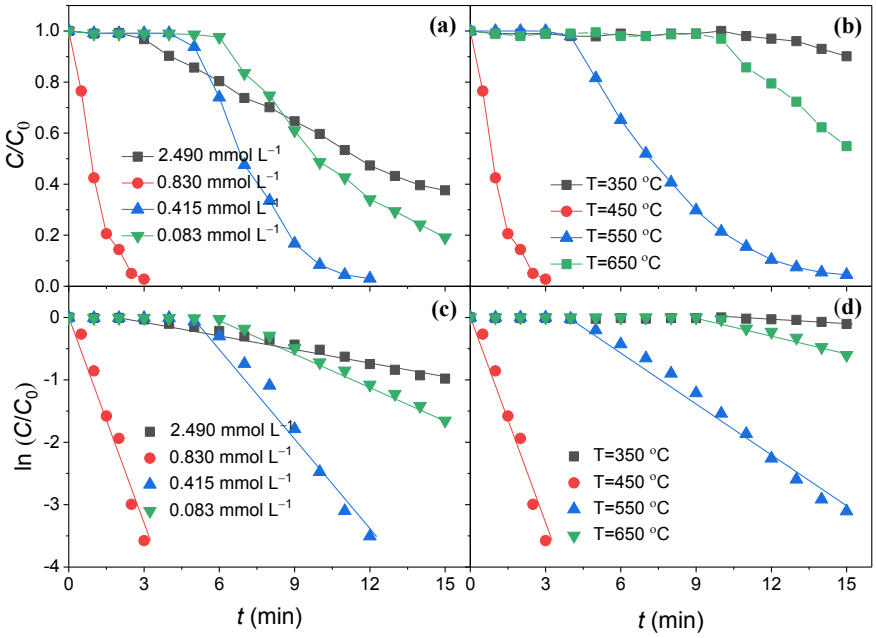

Fig. S4 C/C_0 and $\ln(C/C_0)$ as a function of reaction time over $CNx@Co_3O_4$ prepared using different initial 2,6-diaminopyridine concentrations (a, c) and different carbonization temperatures (b, d). $CNx@Co_3O_4$ loading = 0.05 mg, initial PNP concentration = 0.13 mmol L^{-1} and initial $NaBH_4$ concentration = 0.013 mol L^{-1}.

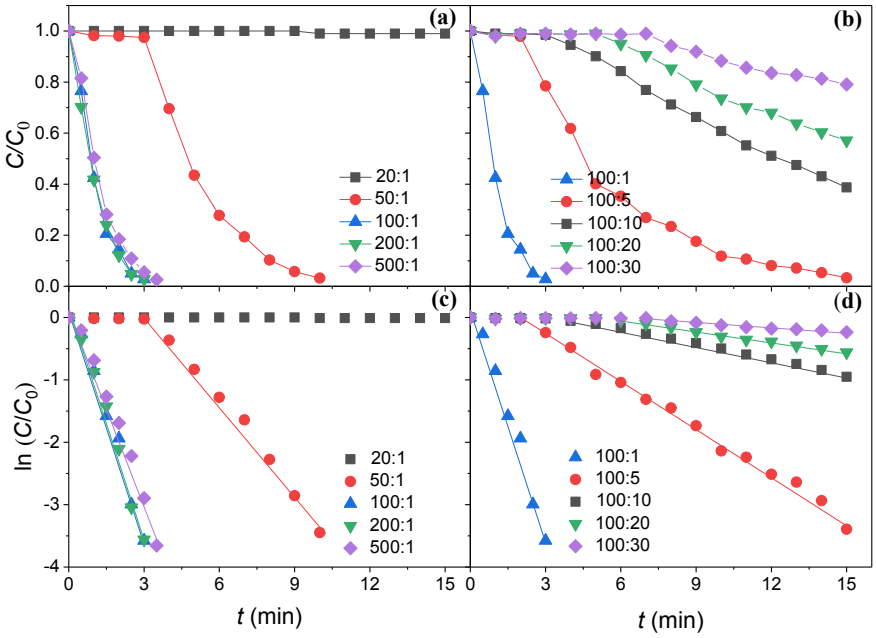

Fig. S5 C/C_0 and $\ln(C/C_0)$ as a function of reaction time over 0.05 mg of $CNx@Co_3O_4$ at different molar ratios of BH_4^-/PNP: (a, c) Initial PNP concentration = 0.13 mmol L^{-1} and (b, d) initial $NaBH_4$ concentration = 0.013 mol L^{-1}.

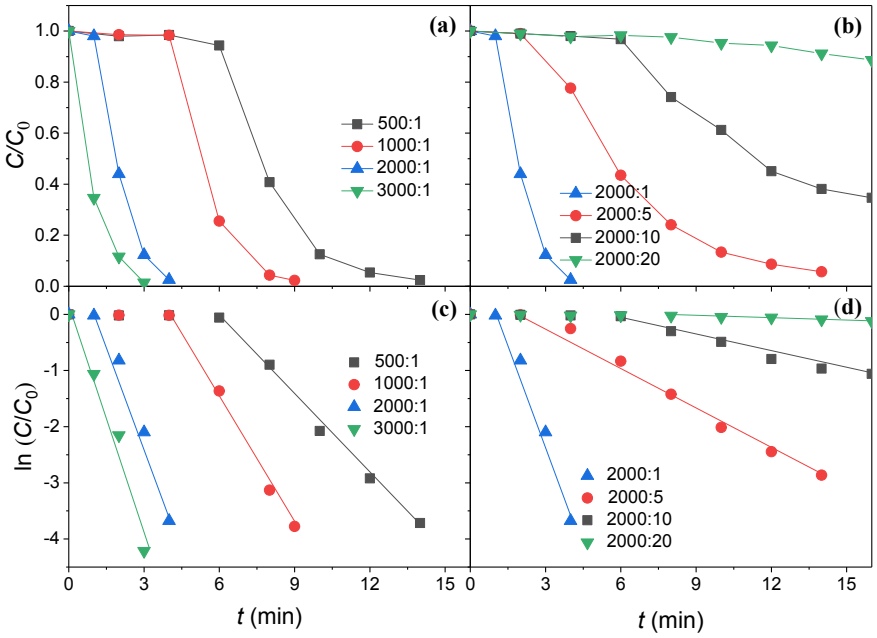

Fig. S6 C/C_0 and $\ln(C/C_0)$ as a function of reaction time over 0.05 mg of Co_3O_4 at different molar ratios of BH_4^-/PNP: (a, c) Initial PNP concentration = 0.13 mmol L^{-1} and (b, d) initial $NaBH_4$ concentration = 0.26 mol L^{-1}.

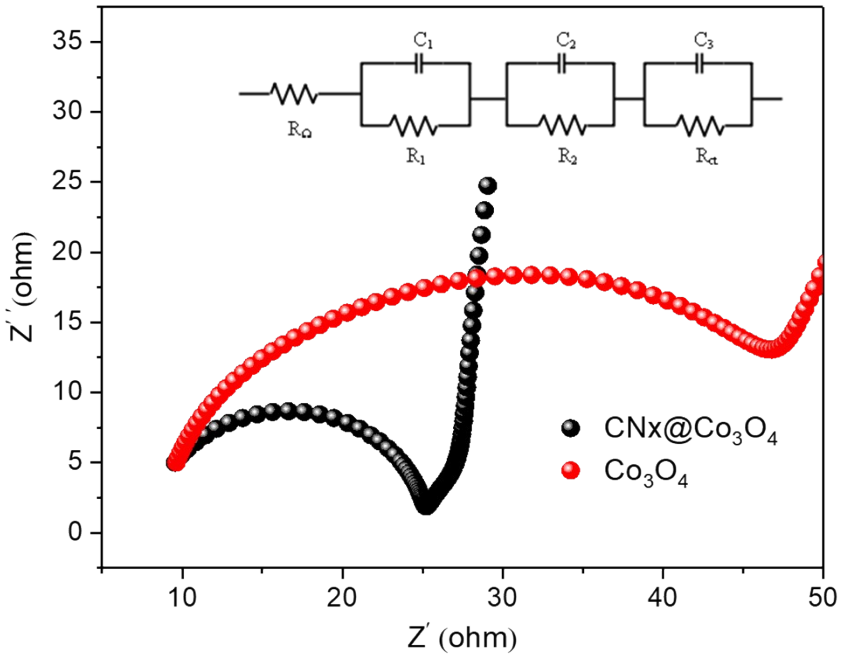

Fig. S7 EIS recorded for CNx@Co_3O_4 and Co_3O_4.

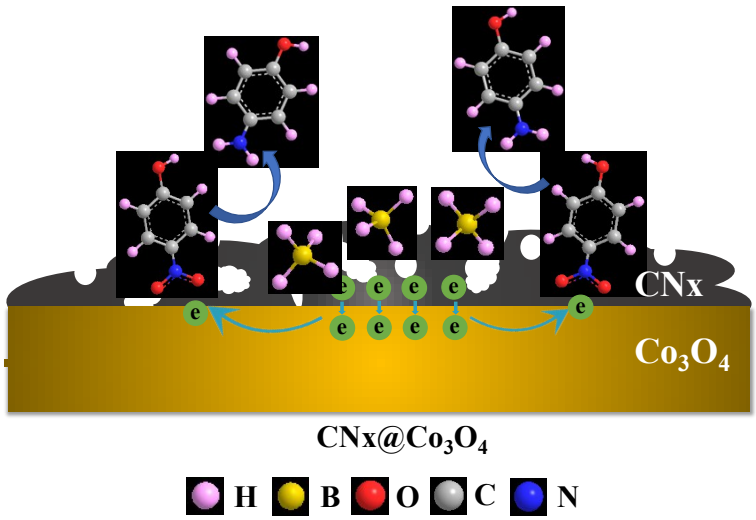

Fig. S8 The possible mechanism for the reduction of PNP to PAP with $NaBH_4$ using the CNx@Co_3O_4 catalyst.

Table S1 A summary of the surface areas and k_{app} values over the different catalysts studied.

Sample	BET ($m^2\ g^{-1}$)	k_{app} (s^{-1})
Co_3O_4	55.4	4.04×10^{-5} (BH_4^-/PNP molar ratio = 100) 0.02 (BH_4^-/PNP molar ratio = 2000)
CNx@Co_3O_4	39.1	0.02 (BH_4^-/PNP molar ratio = 100)
CNx@TiO_2	77.2	1.28×10^{-4} (BH_4^-/PNP molar ratio = 100)
Co_3O_4 + CNx@TiO_2	—	5.03×10^{-5} (BH_4^-/PNP molar ratio = 100)

Table S2 A comparison of the k_{nor} values of CNx@Co_3O_4 with other Co-based and noble metal catalysts reported in the literature.

Catalyst	Experimental conditions	k_{app} (s^{-1})	k_{nor}[a] (s^{-1} g^{-1} L)	Reference
Au ligands	0.000049 g L^{-1} catalyst, 0.1 mmol L^{-1} PNP, 49.95 mmol L^{-1} $NaBH_4$	3.27×10^{-3}	66.67	22
$Au_{53}Pd_{47}$ NPs/GNS	0.0006 g L^{-1} catalyst, 0.05 mmol L^{-1} PNP, 5 mmol L^{-1} $NaBH_4$	0.0145	24.17	23
Ag@AEM	0.01 g L^{-1} catalyst, 0.1 mmol L^{-1} PNP, 10 mmol L^{-1} $NaBH_4$	9.42×10^{-3}	0.921	24
Au/graphene	0.03 g L^{-1} catalyst, 0.093 mmol L^{-1} PNP, 6.66 mmol L^{-1} $NaBH_4$	3.17×10^{-3}	0.11	25
Fe/Cu@Pd	0.15 g L^{-1} catalyst, 0.288 mmol L^{-1} PNP, 10 mmol L^{-1} $NaBH_4$	0.0124	0.08	26
meso-Co_3O_4	0.08 g L^{-1} catalyst, 0.04 mmol L^{-1} PNP, 10 mmol L^{-1} $NaBH_4$	$\sim 3 \times 10^{-4}$	7.5×10^{-3}	27
Co@SiO_2	0.20 g L^{-1} catalyst, 0.60 mmol L^{-1} PNP, 60 mmol L^{-1} $NaBH_4$	0.014	0.07	28
Co-NCC	0.27 g L^{-1} catalyst, 0.168 mmol L^{-1} PNP, 13.4 mmol L^{-1} $NaBH_4$	0.047	0.17	29
Co-NB	0.5 g L^{-1} catalyst, 0.17 mmol L^{-1} PNP, 20 mmol L^{-1} $NaBH_4$	0.009	0.02	8
Reduced Co_3O_4 catalyst	0.071 g L^{-1} catalyst, 0.125 mmol L^{-1} PNP, 12.5 mmol L^{-1} $NaBH_4$	0.025	0.35	1
Au/BNO composite	0.323 g L^{-1} catalyst, 1.62 mmol L^{-1} PNP, 96.77 mmol L^{-1} $NaBH_4$	0.0375	0.116	30
PdPt NTs	0.00044 g L^{-1} catalyst, 0.087 mmol L^{-1} PNP, 2.94 mmol L^{-1} $NaBH_4$	3.33×10^{-3}	1.89	31
CuO@ZIF-67 derivatives	0.015 g L^{-1} catalyst, 0.091 mmol L^{-1} PNP, 18.18 mmol L^{-1} $NaBH_4$	0.069	4.62	32
Co-$CoFe_2O_4$ nanobrush	0.097g L^{-1} catalyst, 0.048 mmol L^{-1} PNP, 64.52 mmol L^{-1} $NaBH_4$	0.0457	0.47	33
CNx@Co_3O_4	0.018 g L^{-1} catalyst, 0.13 mmol L^{-1} PNP, 13 mmol L^{-1} $NaBH_4$	0.020	1.10	This work

[a] The mass-normalized rate constant was calculated based on the catalytic amount.

References

1. H. Chen, M. Yang, S. Tao and G. Chen, *Appl. Catal. B-Environ.*, 2017, **209**, 648-656.

2. T. R. Mandlimath and B. Gopal, *J. Mol. Catal. A-Chem.*, 2011, **350**, 9-15.

3. P. Zhang, C. Shao, Z. Zhang, M. Zhang, J. Mu, Z. Guo and Y. Liu, *Nanoscale*, 2011, **3**, 3357-3363.

4. C. Huang, W. Ye, Q. Liu and X. Qiu, *ACS Appl. Mater. Interfaces*, 2014, **6**, 14469-14476.

5. C. C. Liang, D. F. Cheng, S. J. Ding, P. F. Zhao, M. S. Zhao, X. P. Song and F. Wang, *J. Power Sources*, 2014, **251**, 351-356.

6. Z. Hasan, Y. S. Ok, J. Rinklebe, Y. F. Tsang, D.-W. Cho and H. Song, *J. Alloy. Compd.*, 2017, **703**, 118-124.

7. J. Liu, T. Chen, P. Jian and L. Wang, *Chin. J. Catal.*, 2018, **39**, 1942-1950.

8. D. W. Cho, K. H. Jeong, S. Kim, D. C. W. Tsang, Y. S. Ok and H. Song, *Sci. Total Environ.*, 2018, **612**, 103-110.

9. J. Rong, F. Qiu, T. Zhang, Y. Zhu, J. Xu, Q. Guo and X. Peng, *Appl. Surf. Sci.*, 2018, **447**, 222-234.

10. X. Xu, L. Lai, J. Jiang, Z. He and S. Song, *J. Phys. Chem. C*, 2019, **123**, 9702-9712.

11. E. Pervaiz, M. S. A. Virk, B. Zhang, Y. Conglin and Y. Minghui, *Nanotechnology*, 2017, **28**, 385703.

12. L. Huang, T. Zeng, X. Xu, Z. He, J. Chen and S. Song, *Chem. Eng. J.*, 2019, **372**, 862-872.

13. C. Guo, L. L. Wang, Y. C. Zhu, D. F. Wang, Q. Q. Yang and Y. T. Qian, *Nanoscale*, 2015, **7**, 10123-10129.

14. F. Duarte, F. J. Maldonado-Hodar, A. F. Perez-Cadenas and L. M. Madeira, *Appl.*

Catal. B-Environ., 2009, **85**, 139-147.

15. J.-W. Kim, S. J. Lee, P. Biswas, T. Il Lee and J.-M. Myoung, *Appl. Surf. Sci.*, 2017, **406**, 192-198.

16. X.-X. Ma, X.-Q. He and T. Asefa, *Electrochim. Acta*, 2017, **257**, 40-48.

17. J. Li, Z. Zhou, K. Liu, F. Li, Z. Peng, Y. Tang and H. Wang, *J. Power Sources*, 2017, **343**, 30-38.

18. J. Liu, J. Ke, Y. Li, B. Liu, L. Wang, H. Xiao and S. Wang, *Appl. Catal. B-Environ.*, 2018, **236**, 396-403.

19. X. Pan, X. Gao, X. Chen, H. N. Lee, Y. Liu, R. L. Withers and Z. Yi, *ACS Catal.*, 2017, **7**, 6991-6998.

20. C. Zhu, J. Xu, S. Song, J. Wang, Y. Li, R. Liu and Y. Shen, *Sci. Total Environ.*, 2020, **698**, 134275.

21. Y. Shen, C. Zhu, S. Song, T. Zeng, L. Li and Z. Cai, *Environ. Sci. Technol.*, 2019, **53**, 9091-9101.

22. Y. Dai, P. Yu, X. Zhang and R. Zhuo, *J. Catal.*, 2016, **337**, 65-71.

23. X. Chen, Z. Cai, X. Chen and M. Oyama, *J. Mater. Chem. A*, 2014, **2**, 5668-5674.

24. S. Patra, A. N. Naik, A. K. Pandey, D. Sen, S. Mazumder and A. Goswami, *Appl. Catal. A-Gen.*, 2016, **524**, 214-222.

25. J. Li, C.-y. Liu and Y. Liu, *J. Mater. Chem.*, 2012, **22**, 8426-8430.

26. C. Xu, X. Pan, L. Fang, J. Li and F. Li, *Chem. Eng. J.*, 2019, **360**, 180-189.

27. B. M. Mogudi, P. Ncube and R. Meijboom, *Appl. Catal. B-Environ.*, 2016, **198**, 74-82.

28. N. Yan, Z. Zhao, Y. Li, F. Wang, H. Zhong and Q. Chen, *Inorg. Chem.*, 2014, **53**, 9073-9079.

29. Z. Hasan, D.-W. Cho, C.-M. Chon, K. Yoon and H. Song, *Chem. Eng. J.*, 2016, **298**, 183-190.

30. B. Yu, B. Han, X. Jiang, C. Zhou, K. Xia, Q. Gao and J. Wu, *J. Phys. Chem. C*, 2019, **123**, 10389-10397.

31. Y. Wang, Q. Li, P. Zhang, D. O'Connor, R. S. Varma, M. Yu and D. Hou, *J. Colloid Interface Sci.*, 2019, **539**, 161-167

32. C. Chu, S. Rao, Z. Ma and H. Han, *Appl. Catal. B-Environ.*, 2019, **256**, 117792.

33. Y. Zhang, H. Fang, Y. Zhang, M. Wen, D. Wu and Q. Wu, *J. Colloid Interface Sci.*, 2019, **535**, 499-504.